PAPER

Check for updates

Design, synthesis, molecular docking and anticancer activity of benzothiazolecarbohydrazide–sulfonate conjugates: insights into ROS-induced DNA damage and tubulin polymerization inhibition†

Najla A. Altwaijry, [ID] [a] Mohamed A. Omar,[b] Hanaa S. Mohamed,[c] Marwa M. Mounier,[d] Ahmed H. Afifi[d] and Aladdin M. Srour [ID] *[c]

A series of novel benzothiazolecarbohydrazide–sulfonate conjugates **6a–l** were designed, synthesized, and then assessed as potential antiproliferative agents in three distinct human cancer cell lines: MCF-7 (breast cancer), HCT-116 (colon cancer), and PC3 (prostate cancer), along with a normal cell line (BJ-1). The reference standard used was 5-fluorouracil. The results obtained reveal that the newly synthesized analogs demonstrate varying degrees of cytotoxicity against the targeted cell lines; however, compounds **6i** and **6e** exhibited the highest efficacy against MCF-7, HCT-116, and PC3 cells with IC_{50} values of 78.8 $\pm$ 2.6, 81.4 $\pm$ 1.9, and 90.6 $\pm$ 2.7 μM, respectively, compared to an IC_{50} of 78.4 $\pm$ 4.2 μM for 5-FU in MCF-7 cells, 29.2 $\pm$ 1.7 μM in HCT-116 cells and >200 μM in PC3 cells. Moreover, the most potent compounds demonstrated acceptable safety profiles when evaluated aganist BJ-1 cells. Consequently, compound **6i**, which possesses no cytotoxicity towards BJ-1 cells and displays promising anticancer activity, was further investigated for its impact on tubulin polymerization compared to control MCF-7 cells, 210.3 and 632.9 pg ml^{-1}, respectively. Compound **6i** was found to significantly elevate the ROS levels in treated cancer cells, resulting in an 8.3-fold increase in DNA fragmentation compared to untreated cells. Additionally, it raised the percentage of accumulated cells in the G2 phase from 6.85% to 18.27% in MCF-7 cells. A molecular docking technique was conducted to elucidate the binding energy, binding pose, and binding interactions of compound **6i**, revealing a strong fit within the active sites of the tubulin–colchicine binding site (CBS). This study provides valuable insights into the design and synthesis of novel anticancer agents targeting tubulin polymerization.

[a]Department of Pharmaceutical Sciences, College of Pharmacy, Princess Nourah Bint Abdulrahman University, Riyadh, Saudi Arabia

[b]Chemistry of Natural and Microbial Products Department, Pharmaceutical and Drug Industries Research Institute, National Research Centre, Dokki, 12622, Giza, Egypt

[c]Department of Therapeutic Chemistry, Pharmaceutical and Drug Industries Research Institute, National Research Centre, Dokki, 12622, Giza, Egypt. E-mail: aladdinsrour@gmail.com

[d]Department of Pharmacognosy, Pharmaceutical and Drug Industries Research Institute, National Research Centre, Dokki, 12622, Giza, Egypt

† Electronic supplementary information (ESI) available. See DOI: https://doi.org/10.1039/d4ra07810a

1. Introduction

Cancer is regarded as among the most intricate and challenging illnesses that threaten human life, representing a severe disease burden. According to the latest World Cancer Report, an estimated 20 million new cases were recorded in the year 2020, a number projected to rise to about 30 million by 2030. Due to substantial demographic changes, including population aging and growth, the global number of cancer patients is expected to increase over the next five decades.[1] Different regions will experience varying trends in cancer incidence, further contributing to this rise. Assuming that current incidence patterns for major cancer types continue, we anticipate that the overall cancer incidence will double by 2070 compared to 2020.[2,3] Despite the discovery and approval of various methodologies, techniques, and drugs for cancer treatment, a large number of individuals still endure the burden of this illness each year.[4,5] The adverse impact of off-target effects remains a prominent limitation of cancer therapeutics. As a result, current attention in cancer chemotherapy is directed toward creating highly selective anticancer agents that lack off-target effects. This approach aims to enhance the potency and efficacy specifically against cancer cells while minimizing potential side effects.[5–8] Tubulin polymerization is a vital process for assembling microtubules and is crucial for preserving cell structure and enabling cell division. In various cancers, certain tubulin isoforms can be overexpressed, which may drive tumorigenesis

and accelerate cancer progression.[9–11] Certain cancers, including breast[12,13] and prostate,[14] frequently show over-expression of specific tubulin isoforms, suggesting their significant role in malignancy. Microtubules, essential components of the cytoskeleton with a tubular structure, participate in numerous cellular processes in eukaryotic cells, including processes such as cell growth, transport, communication, movement, replication, and mitotic phase. They are composed of α-tubulin and β-tubulin heterodimers and microtubules are crucial targets for anticancer drugs.[15,16] Drugs that act on microtubules interact with three key regions on tubulin: the paclitaxel location, the vinca zone, and the colchicine region. Inhibitors that focus on the paclitaxel or vinca alkaloid binding areas exhibit multidrug resistance issues and dose-limiting toxicity.[17–19] Consequently, researchers have been increasingly focusing on developing inhibitors that specifically target the colchicine binding site (CBSIs) in recent years.[20,21]

For decades, medicinal chemists have dedicated their efforts to discovering more potent and safer chemotherapeutic agents.[22–24] However, there remains a critical need for anticancer medicines that combine both safety and efficacy. Among various approaches, using heterocyclic scaffolds in drug development has proven highly effective in creating cytotoxic agents. Benzothiazolecarbohydrazide-containing scaffolds are widely recognized for their extensive chemotherapeutic potential, especially as anticancer agents (compound I Fig. 1),[25–27] and as a well-known tubulin polymerization inhibitor which inhibits cell proliferation (compound II Fig. 1).[28–30]

Compounds featuring a sulfonate group have garnered considerable interest from researchers for their potential anticancer properties, as seen with agents like cyclodisone and busulfan (Fig. 1).[31–35] Their unique physicochemical characteristics allow sulfonate-containing structures to effectively interact with lipid membranes, facilitating their passage through cell membranes to target sites.[36,37] N-Acyl hydrazone (NAH) motifs are commonly used in the development of heterocyclic scaffolds of pharmaceutical interest.[38,39] Recently, several compounds containing NAH, including PAC-1 (ref. 40) and LASSBio-1586 (ref. 41) (Fig. 1), have emerged as promising anticancer agents. The strategic incorporation of NAH as a linker is proposed as an inventive methodology to design new potent and versatile anticancer therapies.

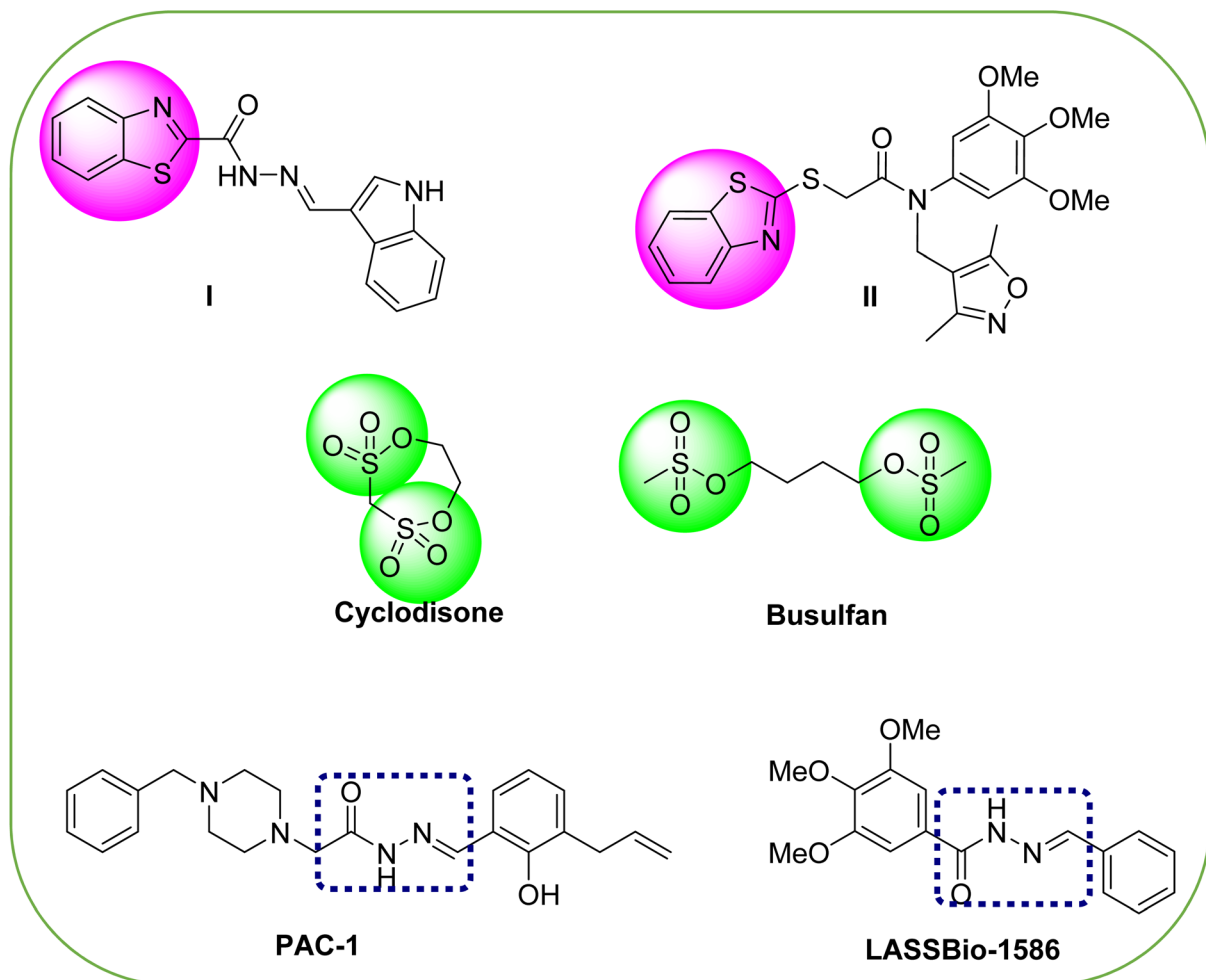Building on our previous studies,[42,43] this research utilizes a structure-based molecular hybridization approach to

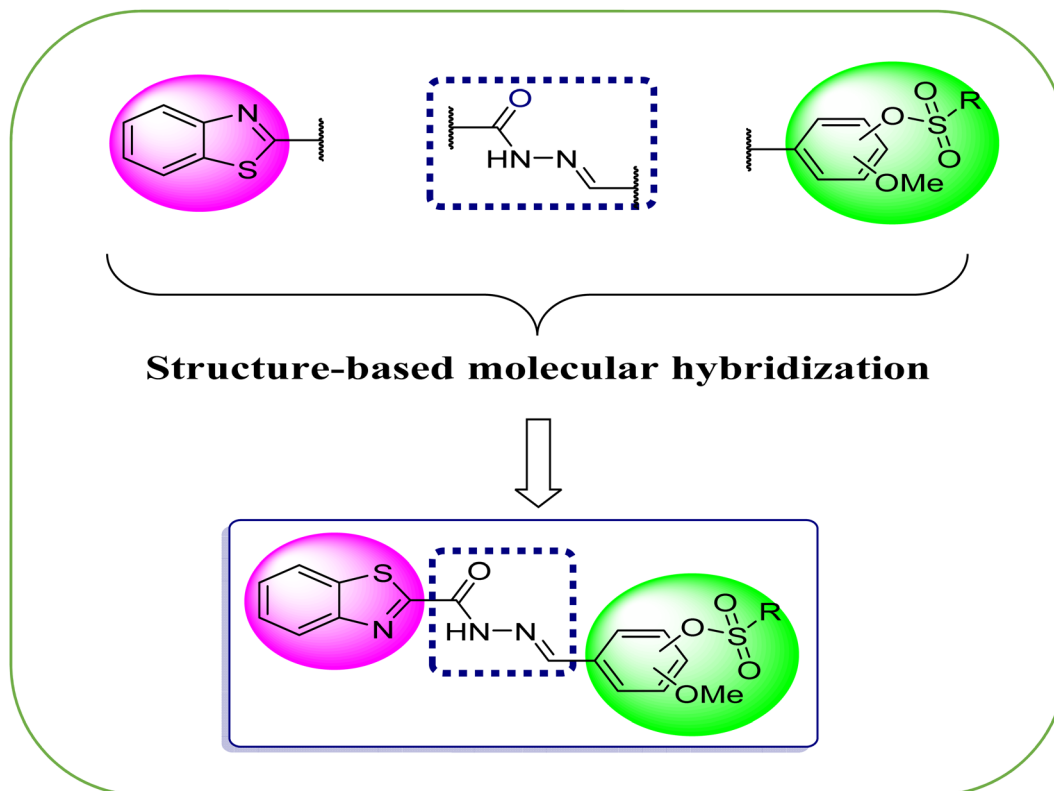Fig. 1 The structures of benzothiazole, sulfonates and N-acyl hydrazone derivatives as anticancer agents.

Fig. 2 The rational design of the targeted benzothiazole–sulfonate conjugates.

efficiently create a series of derivatives with a multi-target action mechanism. We have designed and synthesized various NAH derivatives that incorporate benzothiazole and sulfonate components, aiming to create novel compounds with strong anticancer efficacy, while reducing potential side effects (Fig. 2).

2. Results and discussion
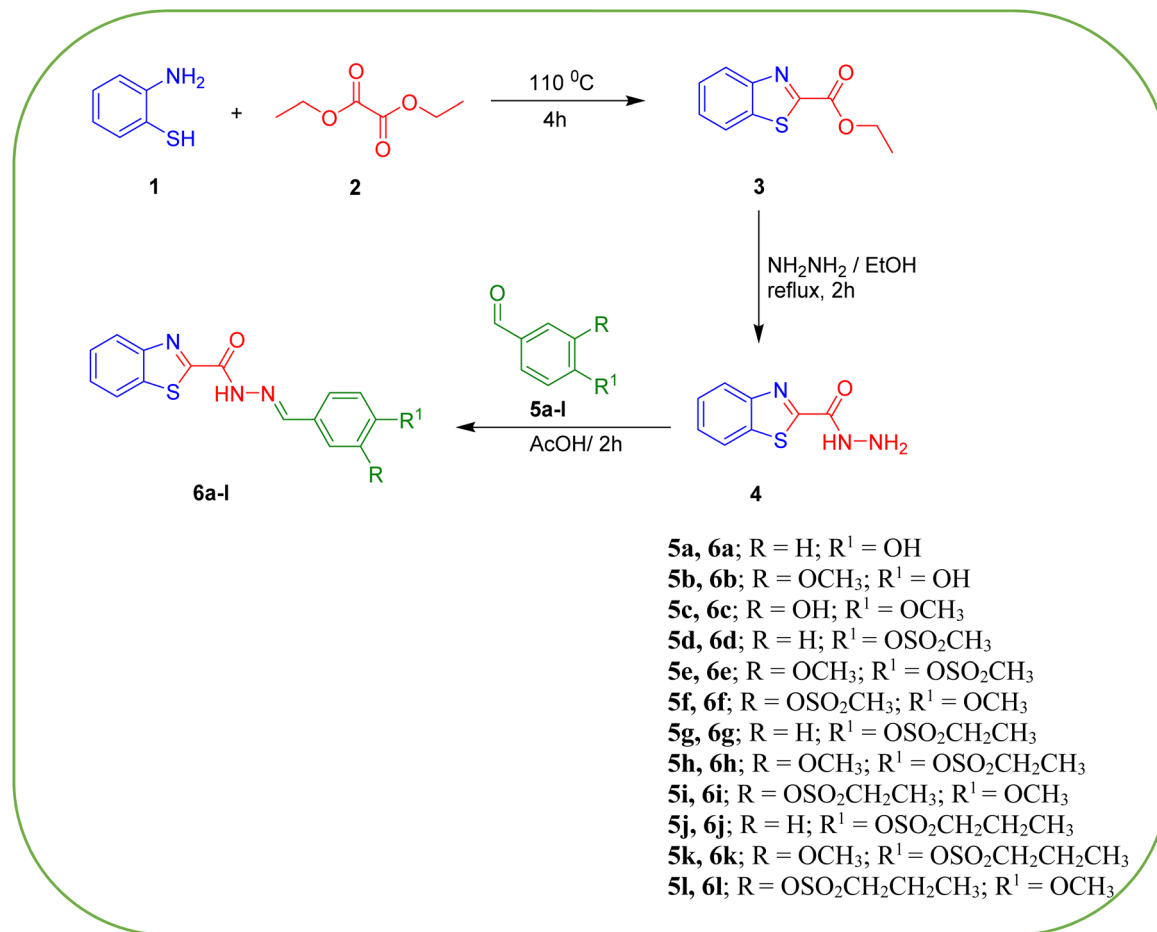
2.1. Chemistry

The synthetic pathway for the production of the desired benzothiazole–sulfonate analogs **6a–l** started from the esterification reaction of 2-amino thiophenol **1** with diethyl oxalate **2** affording the corresponding ester **3**, which is a precursor of benzothiazole carbohydrazide **4** when heated under reflux for 2 h in ethanol with hydrazine monohydrate. Benzothiazole carbohydrazide **4** was then allowed to interact with a variety of *para*-substituted alkane sulfonyl aryl aldehydes **5a–l** to give the targeted benzylidene thiazole carbohydrazide analogs **6a–l** in respectable yields (Scheme 1). The chemical structure of the new chemical entities was proved by employing various spectroscopic methods (IR, ^{1}H NMR and ^{13}C NMR) in addition to the elemental analysis data.

The IR spectrum for derivatives **6a–l** displays at 3371–3210 cm^{-1} strong stretching vibrational bands attributed to NH groups. Additionally, two stretching bands that appeared in the range of 1686–1661 cm^{-1}, and 1665–1641 cm^{-1} are noticed for C=N and C=O groups, respectively, whereas the band representing the sulfonate group SO$_2$ is present in the 1383–1344 cm^{-1} range. The ^{1}H NMR spectrum revealed that the

alkane sulfonate functions (CH$_3$, CH$_3$CH$_2$, and/or CH$_3$CH$_2$CH$_2$) are represented by singlet peaks attributed to methyl groups, triplet and quartet signals attributed to ethyl groups, and triplet, sextet, and triplet signals depicting propyl side chains. The azomethine protons appear as singlet peaks between $\delta_H =$ 8.53 ppm and $\delta_H =$ 8.71 ppm. The NH protons corresponding to the hydrazine derivatives are observed as a singlet peak at $\delta_H =$ 12.78 and 12.46 ppm. The ^{13}C NMR spectrum reveals characteristic peaks associated with the alkane sulfonate groups (CH$_3$, CH$_3$CH$_2$, and/or CH$_3$CH$_2$CH$_2$) in the aliphatic region at $\delta_C =$ 17.00–56.26 ppm. As a representative example of the *para*-substituted alkane sulfonyl analogs **6d–l**, the IR (KBr) spectrum for derivative **6d** disclosed stretching bands at 3224, 1661, 1650, and 1350 cm^{-1}, corresponding to the functional groups NH, C=O, C=N, and SO$_2$, respectively; the ^{1}H NMR spectrum disclosed a singlet peak at $\delta_H =$ 3.44 ppm corresponding to the methyl group and at $\delta_H =$ 7.46–8.28 ppm representing the aromatic region, while the azomethine proton CH=N was depicted at $\delta_H =$ 8.71 ppm, and the NH proton was depicted at $\delta_H =$ 12.76 ppm; ^{13}C NMR exhibited a peak at $\delta_C =$ 37.57 ppm for the methyl group, at $\delta_C =$ 122.73–156.19 ppm representing aromatic carbons and at $\delta_C =$ 163.52 ppm for the C=O group.

2.2. Anticancer activity

The cytotoxic assessment for the new chemical entities was conducted *via* an MTT assay in three distinct human cancer cell lines: MCF-7 (breast cancer), HCT-116 (colon cancer), and PC3 (prostate cancer), along with a normal cell line (BJ-1), beginning

Scheme 1 The synthetic route towards benzothiazole−sulfonate conjugates **6a–l**.

at a concentration of 100 μM. The reference drug 5-fluorouracil was included for comparison. The initial findings indicate that compounds **6c**, **6d**, **6g**, **6i** and **6k** exhibit potent cytotoxicity against MCF-7 cells, with percentages of 58.1, 62.5, 62.3, 53.4, and 59.6, respectively. Similarly, compounds **6d**, **6e**, **6f**, **6g**, **6h**, **6j** and **6k** demonstrated significant effects on HCT-116 cells, with growth inhibition percentages of 66.7, 61.1, 62.8, 68.6, 55.2, 68.5, and 77.2, respectively. For PC3 cells, the most promising compounds were **6d**, **6e**, **6g**, **6h**, **6j** and **6k** with cytotoxic percentages of 66.5, 60.8, 74.8, 63.4, 62.3, and 64.6, respectively.

Conversely, compounds **6a**, **6b**, **6c**, **6i**, and **6l** demonstrated a remarkable safety profile when evaluated in the normal cell line (BJ-1), exhibiting a cytotoxicity percent inhibition ranging from 35% to 10.8% (Table S1 and Fig. S1†).

Based on preliminary cytotoxicity data obtained from both cancer and normal cell lines, only compounds that demonstrated a cytotoxicity percent inhibition of over 50% for all tested cancer cell lines and simultaneously showed a safe profile in the normal cell line (BJ-1) were subjected to dose-dependent screening. The screening involved using a range of concentrations from 100 μM to 12.5 μM to determine their respective IC_{50} values (Table 1).

The findings showed that compound **6i** demonstrated the greatest potency within the tested series against MCF-7, with an IC_{50} value of 78.8 ± 2.6 μM, an almost similar response to the standard reference 5-FU ($IC_{50} = 78.4 \pm 4.2$ μM). Derivative **6c** showed an approximately close IC_{50} value (80.9 ± 3.7) to 5-FU ($IC_{50} = 78.4 \pm 4.2$ μM), while derivatives **6a** ($IC_{50} = 102 \pm 2.1$ μM) and **6e** ($IC_{50} = 81.4 \pm 1.9$ μM) displayed lower activity in the HCT-116 cell line compared to 5-FU ($IC_{50} = 29.2 \pm 1.7$ μM). Furthermore, compound **6e** exhibited promising behavior in the PC3 cell line ($IC_{50} = 90.6 \pm 2.7$ μM) compared to the

Table 1 IC_{50} values of compounds **6a**, **6c**, **6e** and **6i** against three cancer cell lines. SD = standard deviation

Compd ID	IC_{50} values (μM)		
	MCF-7	HCT-116	PC3
6a	—	102 ± 2.1	—
6c	80.9 ± 3.7	—	—
6e	—	81.4 ± 1.9	90.6 ± 2.7
6i	78.8 ± 2.6	—	—
5-FU	78.4 ± 4.2	29.2 ± 1.7	>200

reference standard 5-FU, which displayed an IC_{50} value exceeding 200 μM (Table 1).

Based on the findings that we observed and following the SAR (structure-activity relationship) rule, it was discovered that incorporating an alkane sulfonate moiety significantly enhanced the cytotoxic activity in all examined cell lines, except for compound **6l**. Notably, an activity order was observed, with methane > ethane > propane, which holds promise for guiding the future design of potent anti-cancer candidates. This information will be valuable for developing effective strategies to pursue novel anti-cancer agents. Except for compounds **6d**, **6f**, **6g**, **6h**, **6j** and **6k**, the series demonstrated no to minimal cytotoxic activity detected against the used normal human cell line (BJ-1).

2.3. Tubulin evaluation of *in vitro* tubulin polymerization inhibitory activity

Antitubulin-targeting therapies are considered a good strategy for fighting cancer cells. Tubulin-microtubules hold a crucial role in cell survival. The polymerization of α- and β-tubulin dimers forms microtubules, while their depolymerization reverts them to tubulin dimers. Disrupting microtubule dynamics affects DNA segregation and cell mitosis, leading to the destruction of cancer cells.[44] To explore the relationship between the newly synthesized derivatives and tubulin in terms of their antiproliferative activity, compound **6i**, the most potent, was examined for its tubulin polymerization properties compared with the control MCF7 cells. The assay revealed that **6i** influenced the microtubule mass protein tubulin B by preventing the formation of tubulin polymers in MCF-7 as compared to untreated breast cells with 210.3 and 632.9 pg ml^{-1}, respectively (Fig. S2†).

2.4. Reactive oxygen species (ROS) production

Extensive research has been conducted on generating intracellular oxidative stress in the form of reactive oxygen species (ROS) in various kinds of cancer.[45] ROS-stimulating agents may enable specific cancer therapy. The maintenance of various cellular processes relies on redox homeostasis. Cancer cells generally display elevated levels of reactive oxygen species (ROS) while maintaining redox balance due to their antioxidant capacity. Recent studies have focused on targeting cancer cells by increasing ROS levels and disrupting redox balance, leading

to significant damage to the cancer cells.[46] The levels of intracellular ROS have been assessed to check whether compound **6i**-mediated membrane damage can lead to oxidative stress induction. It was observed that **6i** manages to elevate ROS levels in treated cancer cells, leading to the induction of DNA fragmentation by 8.3 fold compared to untreated cells (Fig. S3†).

2.5. Cell cycle analysis

Most cytotoxic drugs produce cell cycle arrest, either directly through regulating cell cycle regulators or indirectly by modifying other cell components. To investigate the effects of derivative **6i** on the cell cycle. The MCF-7 cells were subjected to a 24 h treatment with **6i**. Following this treatment, the cells were marked with propidium iodide (PI) and subsequently examined *via* flow cytometry. The findings indicated an increase in the proportion of cells in the G2 phase, rising from 6.85% in the untreated control group to 18.27% in the group treated with **6i**. This observation implies that compound **6i** induces a cell cycle halt in MCF-7 cells at the G2/M stage (Fig. 3).

2.6. Cell apoptosis

Mitochondria are involved in many vital cellular processes, like differentiation and apoptosis. Mitochondria-targeting therapy might be more operatively related to conventional chemotherapy. Mitochondrial dysfunction leads to apoptosis initiation.[47] Apoptosis is a physiological process that holds a key role in maintaining tissue homeostasis, and it is considered to be the most appropriate way of eliminating undesirable cells. Most existing anticancer drugs are mediated by the initiation of apoptosis in cancer cells.

To further inspect the impact of compound **6i** against MCF-7 tumour cells, the capability of **6i** to induce apoptosis was inspected by flow cytometry. Treatment of MCF-7 cells with the predetermined IC_{50} of **6i** induced necrosis (Fig. 4). The early apoptosis increases from 0.37% (control) to 13.88% (treated cells) and late apoptosis increases from 0.14% (control) to 7.31% (treated cells). Compound **6i** specifically induced necrosis in the treated MCF-7 cells, unlike the controls.

2.7. Molecular docking study

Molecular docking simulation was used to investigate how derivative **6i** interacts with the binding site of colchicine (CBS) on tubulin. Specifically, the compound's binding energy, spatial
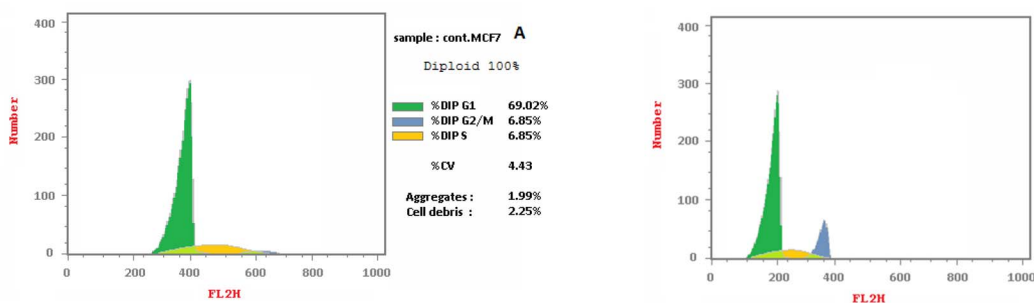

Fig. 3 Cell cycle analysis of the MCF-7 cell line after 24 hours of treatment with **6i**. Analysis was done by annexin V/PI staining.
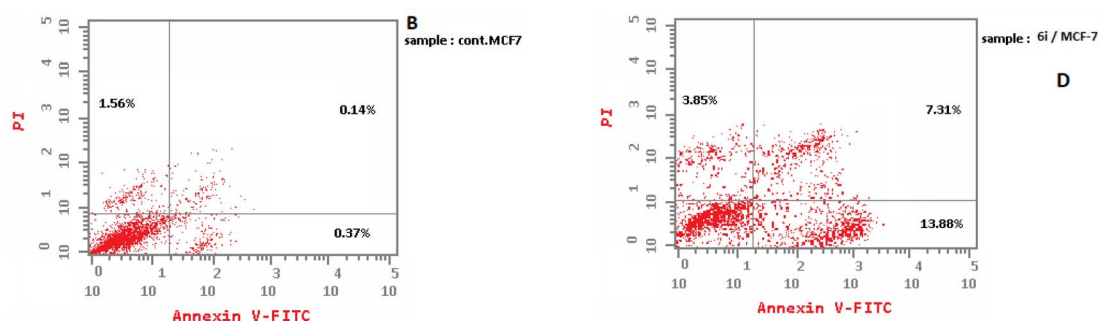
Fig. 4 Compound 6i induced cell apoptosis in an annexin V-FITC assay. It represents the total of early apoptotic (annexin V$^+$/PI$^-$) cell percentage and late apoptotic (annexin V$^+$/PI$^+$) cell percentage.

orientation, and interaction mechanisms at this unique pocket, which is strategically positioned at the interface between the α and β tubulin protein complex subunits, were analyzed. CBS is reported to encompass three distinct interaction zones. Zone 1 is the most proximal to the α–β tubulin interface and zone 2 is located next to zone 1 in the β-tubulin subunit, while zone 3 is

extra severely submerged in β-tubulin. Zone 2 is considered the main zone which accommodates the major portion of the inhibitor structures. In contrast, both zone 1 and zone 3 act as "accessory zones" that help stabilize the inhibitor inside the binding pocket.[48] Tubulin CBS inhibitors exhibit different orientations and localizations within CBS, corresponding to the
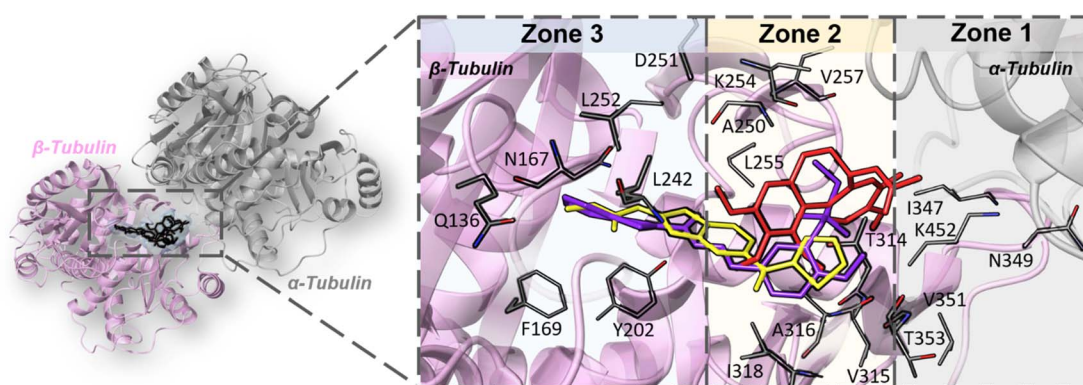

Fig. 5 3D depiction illustrating different binding modes of colchicine (red sticks), nocodazole (yellow sticks) and compound 6i (purple sticks) inside tubulin CBS.
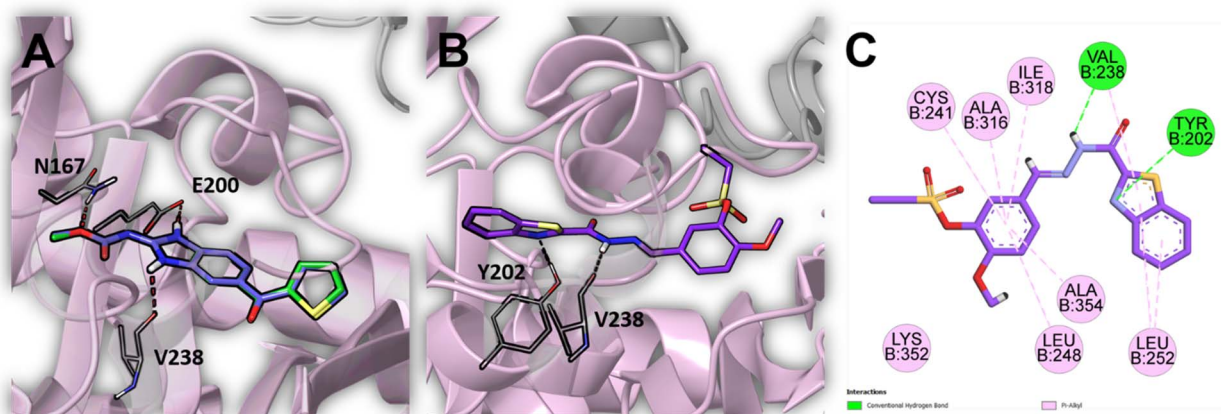

Fig. 6 (A) Superposition of the co-crystalized pose (green sticks) and docked pose (purple sticks) of nocodazole inside tubulin CBS. (B) 3D depiction illustrating the docking pose of 6i inside tubulin CBS. (C) 2D presentation of the binding interactions between 6i and tubulin CBS residues.

three identified zones. Classical CBS inhibitors, such as colchicine, are found in zone 1 and zone 2 near the α-tubulin subunit, while non-classical CBS inhibitors, like nocodazole, penetrate more deeply into zone 2 and zone 3 (Fig. 5).[49] To validate our docking protocol, we redocked the co-crystalized inhibitor (nocodazole) into the tubulin CBS and compared the docked pose with the original co-crystalized pose. The docking protocol managed to reproduce the co-crystalized pose as indicated by the perfect superposition and low RMSD value (0.16 Å) between the two poses (Fig. 6A). Compound **6i** has demonstrated strong binding to tubulin CBS as shown by its docking score (−9.93 kcal mol⁻¹), which surpasses that of nocodazole and colchicine (−8.53 and −8.32 kcal mol⁻¹, respectively). Compound **6i** has adopted a binding mode similar to nocodazole as it was placed in zone 2 extending in zone 3 deeply in β-tubulin (Fig. 5). It is important to note that the *o*-methoxy phenyl ethane sulfonate ring does not directly interact with the binding pocket; instead, it is located in the hydrophobic pocket of zone 2 forming several hydrophobic pi–alkyl interactions with Cys241, Leu248, Ala316, Ile318, and Ala354, this may potentially inhibit the normal dimerization of tubulin subunits. Conversely, the benzothiazole ring is deeply inserted into zone 3, forming two hydrogen bonds: one among the nitrogen atom of benzothiazole besides Tyr202, and another between hydrazone (NH) and Val238. Additionally, hydrophobic pi–alkyl interactions are observed between the benzothiazole ring and both Leu252 and Val238 (Fig. 6B and C).

3. Experimental

3.1. Chemistry

The ESI† file includes comprehensive details on the chemicals, various analytical equipment, and spectral charts displayed in Fig. S4–S27.†

3.1.1. General procedure for the preparation of the new derivatives 6a–l.
The synthetic protocol involved interacting benzo[*d*]thiazole-2-carbohydrazide (**4**) with *para*-substituted alkane sulfonyl aryl aldehydes (**5a–i**) under reflux conditions in glacial acetic acid. The reaction was tracked using thin-layer chromatography and allowed to proceed for 2–4 h. After cooling, the reaction mixture was quenched with ice-cold water, resulting in a precipitate. This precipitate was then separated by filtration, dried, and recrystallized in ethanol to yield colorless microcrystalline derivatives **6a–l**.

3.1.1.1. N′-(4-Hydroxybenzylidene)benzo[d]thiazole-2-carbohydrazide (6a). Yield: 98%; mp 285–257 °C; IR (KBr) cm⁻¹, *v*: 3400 (OH), 3312 (NH), 1686 (C=O), 1650 (C=N); ¹H NMR δ (ppm): 6.86 (d, 2H, *J* = 9.0 Hz, H-3′ and H-5′), 7.57 (d, 2H, *J* = 9.0 Hz, H-2′ and H-6′), 7.61–7.62 (m, 1H, H-5), 7.64–7.67 (m, 1H, H-6), 8.18 (d, 1H, *J* = 8.5 Hz, H-4), 8.26 (d, 1H, *J* = 8.5 Hz, H-7), 8.57 (s, 1H, CH=N), 10.02 (brs, 1H, OH), 12.46 (s, 1H, NH); ¹³C NMR δ (ppm): 115.76 (C-3′ and C-5′), 122.97 (C-4), 123.98 (C-5), 124.96 (C-1′), 162.96 (C-6), 127.17 (C-7), 129.18 (C-2′ and C-6′), 135.99 (C-7a), 150.81 (C=N), 152.70 (C-3a), 155.78 (C-4′), 159.82 (C-2), 163.98 (C=O); anal. calcd for: C₁₅H₁₁N₃O₂S (297.33): C, 60.59; H, 3.73; N, 14.13. Found: C, 60.71; H, 3.51; N, 14.29.

3.1.1.2. N′-(4-Hydroxy-3-methoxybenzylidene)benzo[d]thiazole-2-carbohydrazide (6b). Yield: 91%; mp 232–234 °C; IR (KBr) cm⁻¹, *v*: 3488 (OH), 3304 (NH), 1656 (C=O), 1641 (C=N); ¹H NMR δ (ppm): 3.84 (s, 3H, OCH₃), 6.87 (d, 1H, *J* = 8.0 Hz, H-5′), 7.11 (d, 1H, *J* = 8.0 Hz, H-6′), 7.33 (d, 1H, *J* = 1.0 Hz, H-2′), 7.58–7.60 (m, 1H, H-5), 7.63–7.66 (m, 1H, H-6), 8.17 (d, 1H, *J* = 8.0 Hz, H-4), 8.24 (d, 1H, *J* = 8.0 Hz, H-7), 8.57 (s, 1H, CH=N), 9.64 (brs, 1H, OH), 12.48 (brs, 1H, NH); ¹³C NMR δ (ppm): 55.61 (CH₃), 109.29 (C-2′), 115.56 (C-5′), 122.74 (C-4), 122.80 (C-5), 124.04 (C-6′), 125.47 (C-6), 127.00 (C-7), 127.21 (C-1′), 136.07 (C-7a), 148.14 (C=N), 149.54 (C-3′), 151.17 (C-4′), 152.76 (C-3a), 155.95 (C-2), 163.96 (C=O); anal. calcd for: C₁₆H₁₃N₃O₃S (327.36): C, 58.71; H, 4.00; N, 12.84. Found: C, 58.55; H, 4.22; N, 12.70.

3.1.1.3. N′-(3-Hydroxy-4-methoxybenzylidene)benzo[d]thiazole-2-carbohydrazide (6c). Yield: 78%; mp 250–252 °C; IR (KBr) cm⁻¹, *v*: 3461 (OH), 3210 (NH), 1676 (C=O), 1649 (C=N); ¹H NMR δ (ppm): 3.81 (s, 3H, OCH₃), 6.98 (d, 1H, *J* = 8.5 Hz, H-5′), 7.07 (dd, 1H, *J* = 8.5, 1.5 Hz, H-6′), 7.31 (d, 1H, *J* = 2.0 Hz, H-2′), 7.58–7.61 (m, 1H, H-5), 7.64–7.67 (m, 1H, H-6), 8.18 (d, 1H, *J* = 8.5 Hz, H-4), 8.25 (d, 1H, *J* = 8.5 Hz, H-7), 8.53 (s, 1H, CH=N), 9.37 (s, 1H, OH), 12.50 (s, 1H, NH); ¹³C NMR δ (ppm): 55.56 (CH₃), 111.85 (C-5′), 112.51 (C-2′), 120.80 (C-4), 122.94 (C-6′), 124.00 (C-5), 126.87 (C-6), 126.96 (C-7), 127.17 (C-1′), 136.04 (C-7a), 146.97 (C=N), 150.21 (C-3′), 150.71 (C-4′), 152.72 (C-3a), 155.89 (C-2), 163.93 (C=O); anal. calcd for: C₁₆H₁₃N₃O₃S (327.36): C, 58.71; H, 4.00; N, 12.84. Found: C, 58.90; H, 4.21; N, 12.69.

3.1.1.4. 4-((2-(Benzo[d]thiazole-2-carbonyl)hydrazono)methyl)phenyl methanesulfonate (6d). Yield: 76%; mp 219–221 °C; IR (KBr) cm⁻¹, *v*: 3224 (NH), 1661 (C=O), 1650 (C=N), 1350 (SO₂); ¹H NMR δ (ppm): 3.44 (s, 3H, CH₃), 7.46 (d, 2H, *J* = 9.0 Hz, H-3′ and H-5′), 7.61–7.64 (m, 1H, H-5), 7.65–7.69 (m, 1H, H-6), 7.85 (d, 2H, *J* = 9.0 Hz, H-2′ and H-6′), 8.20 (d, 1H, *J* = 9.0 Hz, H-4), 8.28 (d, 1H, *J* = 8.5 Hz, H-7), 8.71 (s, 1H, CH=N), 12.76 (s, 1H, NH); ¹³C NMR δ (ppm): 37.57 (CH₃), 122.73 (C-2′ and C-6′), 123.01 (C-4), 124.05 (C-6), 127.10 (C-7), 127.24 (C-5), 128.99 (C-3′ and C-5′), 133.04 (C-4′), 136.03 (C-7a), 149.13 (C=N), 150.29 (C-3a), 152.64 (C-1′), 156.19 (C-2), 163.52 (C=O); anal. calcd for: C₁₆H₁₃N₃O₄S₂ (375.42): C, 51.19; H, 3.49; N, 11.19. Found: C, 51.25; H, 3.31; N, 11.09.

3.1.1.5. 4-((2-(Benzo[d]thiazole-2-carbonyl)hydrazono)methyl)-2-methoxyphenyl methanesulfonate (6e). Yield: 80%; mp 185–187 °C; IR (KBr) cm⁻¹, *v*: 3362 (NH), 1671 (C=O), 1665 (C=N), 1361 (SO₂); ¹H NMR δ (ppm): 3.39 (s, 3H, CH₃), 3.94 (s, 3H, OCH₃), 7.35 (d, 1H, *J* = 8.5 Hz, H-6′), 7.42 (d, 1H, *J* = 9.0 Hz, H-5′), 7.52 (s, 1H, H-3′), 7.61–7.64 (m, 1H, H-5), 7.66–7.69 (m, 1H, H-6), 8.21 (d, 1H, *J* = 9.0 Hz, H-4), 8.28 (d, 1H, *J* = 8.0 Hz, H-7), 8.67 (s, 1H, CH=N), 12.78 (s, 1H, NH); ¹³C NMR δ (ppm): 38.46 (CH₃), 56.08 (OCH₃), 110.84 (C-3′), 120.74 (C-4), 123.01 (C-6′), 124.11 (C-6), 124.32 (C-7), 127.14 (C-5′), 127.27 (C-5), 134.11 (C-4′), 136.08 (C-7a), 139.36 (C-1′), 149.44 (C=N), 151.79 (C-2′), 152.68 (C-3a), 156.29 (C-2), 163.52 (C=O); anal. calcd for: C₁₇H₁₅N₃O₅S₂ (405.44): C, 50.36; H, 3.73; N, 10.36. Found: C, 50.21; H, 3.51; N, 10.49.

3.1.1.6. 5-((2-(Benzo[d]thiazole-2-carbonyl)hydrazono)methyl)-2-methoxyphenyl methanesulfonate (6f). Yield: 99%; mp 221–223 °C; IR (KBr) cm⁻¹, *v*: 3349 (NH), 1670 (C=O), 1659 (C=

N), 1363 (SO$_2$); ^{1}H NMR δ (ppm): 3.40 (s, 3H, CH$_3$), 3.92 (s, 3H, OCH$_3$), 7.31 (d, 1H, J = 8.5 Hz, H-6′), 7.31 (d, 1H, J = 8.5 Hz, H-3′), 7.60–7.63 (m, 1H, H-5), 7.65–7.69 (m, 3H, H-6 + H4′ + H6′), 8.20 (d, 1H, J = 8.0 Hz, H-4), 8.27 (d, 1H, J = 8.0 Hz, H-7), 8.62 (s, 1H, CH=N), 12.68 (s, 1H, NH); ^{13}C NMR δ (ppm): 38.38 (CH$_3$), 56.26 (OCH$_3$), 113.77 (C-3′), 121.94 (C-6′), 122.97 (C-7), 124.05 (C-4′), 127.05 (C-4 + C-5), 127.21 (C-6), 128.03 (C-5′), 136.05 (C-3a), 136.07 (C-1′), 149.12 (C=N), 152.69 (C-7a), 153.17 (C-1′), 156.08 (C-2), 163.67 (C=O); anal. calcd for: C$_{17}$H$_{15}$N$_3$O$_5$S$_2$ (405.44): C, 50.36; H, 3.73; N, 10.36. Found: C, 50.29; H, 3.91; N, 10.22.

3.1.1.7. 4-((2-(Benzo[d]thiazole-2-carbonyl)hydrazono)methyl) phenyl ethanesulfonate (6g). Yield: 72%; mp 191–193 °C; IR (KBr) cm^{-1}, ν: 3320 (NH), 1681 (C=O), 1660 (C=N), 1355 (SO$_2$); ^{1}H NMR δ (ppm): 1.39 (t, 3H, J = 7.0 Hz, CH$_3$), 3.58 (q, 2H, J = 7.0 Hz, CH$_2$), 7.44 (d, 2H, J = 8.5 Hz, H-3′ and H-5′), 7.60–7.63 (m, 1H, H-5), 7.65–7.68 (m, 1H, H-6), 7.85 (d, 2H, J = 8.5 Hz, H-2′ and H-6′), 8.20 (d, 1H, J = 8.0 Hz, H-4), 8.27 (d, 1H, J = 7.5 Hz, H-7), 8.70 (s, 1H, CH=N), 12.75 (s, 1H, NH); ^{13}C NMR δ (ppm): 8.00 (CH$_3$), 44.83 (CH$_2$), 122.61 (C-2′ and C-6′), 122.99 (C-4), 124.04 (C-6), 127.08 (C-7), 127.22 (C-5), 128.99 (C-3′ and C-5′), 132.93 (C-4′), 136.04 (C-7a), 149.11 (C=N), 150.13 (C-3a), 152.64 (C-1′), 156.19 (C-2), 163.53 (C=O); anal. calcd for: C$_{17}$H$_{15}$N$_3$O$_4$S$_2$ (389.44): C, 52.43; H, 3.88; N, 10.79. Found: C, 52.61; H, 3.61; N, 10.61.

3.1.1.8. 4-((2-(Benzo[d]thiazole-2-carbonyl)hydrazono) methyl)-2-methoxyphenyl ethanesulfonate (6h). Yield: 78%; mp 175–177 °C; IR (KBr) cm^{-1}, ν: 3299 (NH), 1681 (C=O), 1659 (C=N), 1383 (SO$_2$); ^{1}H NMR δ (ppm): 1.40 (t, 3H, J = 6.5 Hz, CH$_3$), 3.53 (q, 2H, J = 7.0 Hz, CH$_2$), 3.92 (s, 3H, OCH$_3$), 7.34 (d, 1H, J = 8.0 Hz, H-6′), 7.40 (d, 1H, J = 8.0 Hz, H-5′), 7.51 (s, 1H, H-3′), 7.61–7.64 (m, 1H, H-5), 7.66–7.69 (m, 1H, H-6), 8.21 (d, 1H, J = 7.5 Hz, H-4), 8.27 (d, 1H, J = 8.0 Hz, H-7), 8.67 (s, 1H, CH=N), 12.76 (s, 1H, NH); ^{13}C NMR δ (ppm): 8.04 (CH$_3$), 45.76 (CH$_2$), 56.08 (OCH$_3$), 110.80 (C-3′), 120.69 (C-4), 123.02 (C-6′), 124.09 (C-6), 124.26 (C-7), 127.13 (C-5′), 127.26 (C-5), 133.96 (C-4′), 136.07 (C-7a), 139.28 (C-1′), 149.42 (C=N), 151.74 (C-2′), 152.67 (C-3a), 156.26 (C-2), 163.54 (C=O); anal. calcd for: C$_{18}$H$_{17}$N$_3$O$_5$S$_2$ (419.47): C, 51.54; H, 4.09; N, 10.02. Found: C, 51.71; H, 4.21; N, 10.15.

3.1.1.9. 5-((2-(Benzo[d]thiazole-2-carbonyl)hydrazono) methyl)-2-methoxyph-enyl ethanesulfonate (6i). Yield: 65%; mp 215–217 °C; IR (KBr) cm^{-1}, ν: 3367 (NH), 1678 (C=O), 1656 (C=N), 1351 (SO$_2$); ^{1}H NMR δ (ppm): 1.41 (t, 3H, J = 7.5 Hz, CH$_3$), 3.54 (q, 2H, J = 7.5 Hz, CH$_2$), 3.91 (s, 3H, OCH$_3$), 7.31 (d, 1H, J = 9.0 Hz, H-3′), 7.60–7.63 (m, 1H, H-5), 7.65–7.68 (m, 3H, H-6 + H-4′ + H6′), 8.20 (d, 1H, J = 8.0 Hz, H-4), 8.27 (d, 1H, J = 8.0 Hz, H-7), 8.61 (s, 1H, CH=N), 12.67 (s, 1H, NH); ^{13}C NMR δ (ppm): 8.00 (CH$_3$), 45.69 (CH$_2$), 56.24 (OCH$_3$), 113.68 (C-3′), 121.77 (C-6′), 122.98 (C-7), 124.02 (C-4′), 126.98 (C-4), 127.04 (C-5), 127.20 (C-6), 127.94 (C-5′), 136.01 (C-3a), 137.93 (C-1′), 149.10 (C=N), 152.66 (C-7a), 153.10 (C-1′), 156.03 (C-2), 163.66 (C=O); anal. calcd for: C$_{18}$H$_{17}$N$_3$O$_5$S$_2$ (419.47): C, 51.54; H, 4.09; N, 10.02. Found: C, 51.37; H, 4.18; N, 10.13.

3.1.1.10. 4-((2-(Benzo[d]thiazole-2-carbonyl)hydrazono) methyl)phenyl propane-1-sulfonate (6j). Yield: 65%; mp 176–178 °C; IR (KBr) cm^{-1}, ν: 3371 (NH), 1679 (C=O), 1658 (C=N), 1359 (SO$_2$); ^{1}H NMR δ (ppm): 1.04 (s, 3H, J = 7.5 Hz, CH$_3$), 1.86 (sextet, 2H, J = 7.5 Hz, CH$_2$), 3.55 (t, 2H, J = 8.0 Hz, CH$_2$), 7.43 (d, 2H, J = 9.0 Hz, H-3′ and H-5′), 7.60–7.63 (m, 1H, H-5), 7.65–7.69 (m, 1H, H-6), 7.84 (d, 2H, J = 9.0 Hz, H-2′ and H-6′), 8.20 (d, 1H, J = 8.5 Hz, H-4), 8.27 (d, 1H, J = 8.5 Hz, H-7), 8.70 (s, 1H, CH=N), 12.75 (s, 1H, NH); ^{13}C NMR δ (ppm): 12.29 (CH$_3$), 16.94 (CH$_2$), 51.52 (CH$_2$), 122.62 (C-2′ and C-6′), 122.97 (C-4), 124.04 (C-6), 127.06 (C-7), 127.20 (C-5), 128.98 (C-3′ and C-5′), 132.92 (C-4′), 136.04 (C-7a), 149.11 (C=N), 150.11 (C-3a), 152.64 (C-1′), 156.18 (C-2), 163.53 (C=O); anal. calcd for: C$_{18}$H$_{17}$N$_3$O$_4$S$_2$ (403.47): C, 53.58; H, 4.25; N, 10.41. Found: C, 53.81; H, 4.11; N, 10.60.

3.1.1.11. 4-((2-(Benzo[d]thiazole-2-carbonyl)hydrazono) methyl)-2-methoxyphenyl propane-1-sulfonate (6k). Yield: 66%; mp 150–152 °C; IR (KBr) cm^{-1}, ν: 3340 (NH), 1674 (C=O), 1651 (C=N), 1344 (SO$_2$); ^{1}H NMR δ (ppm): 1.04 (t, 3H, J = 7.5 Hz, CH$_3$), 1.88 (sextet, 2H, J = 7.5 Hz, CH$_2$), 3.50 (t, 2H, J = 8.0 Hz, CH$_2$), 3.93 (s, 3H, OCH$_3$), 7.34 (d, 1H, J = 8.0 Hz, H-6′), 7.40 (d, 1H, J = 8.0 Hz, H-5′), 7.51 (s, 1H, H-3′), 7.61–7.64 (m, 1H, H-5), 7.66–7.69 (m, 1H, H-6), 8.21 (d, 1H, J = 8.0 Hz, H-4), 8.28 (d, 1H, J = 8.0 Hz, H-7), 8.67 (s, 1H, CH=N), 12.77 (s, 1H, NH); ^{13}C NMR δ (ppm): 12.36 (CH$_3$), 17.02 (CH$_2$), 52.44 (CH$_2$), 56.07 (OCH$_3$), 110.78 (C-3′), 120.66 (C-4), 123.00 (C-6′), 124.06 (C-6), 124.29 (C-7), 127.10 (C-5′), 127.24 (C-5), 133.93 (C-4′), 136.04 (C-7a), 139.24 (C-1′), 149.39 (C=N), 151.71 (C-2′), 152.65 (C-3a), 156.22 (C-2), 163.53 (C=O); anal. calcd for: C$_{19}$H$_{19}$N$_3$O$_5$S$_2$ (433.50): C, 52.64; H, 4.42; N, 9.69. Found: C, 52.71; H, 4.29; N, 9.50.

3.1.1.12. 5-((2-(Benzo[d]thiazole-2-carbonyl)hydrazono) methyl)-2-methoxyphenyl propane-1-sulfonate (6l). Yield: 70%; mp 210–212 °C; IR (KBr) cm^{-1}, ν: 3371 (NH), 1673 (C=O), 1648 (C=N), 1353 (SO$_2$); ^{1}H NMR δ (ppm): 1.05 (t, 3H, J = 7.5 Hz, CH$_3$), 1.88 (sextet, 2H, J = 7.5 Hz, CH$_2$), 3.51 (t, 2H, J = 7.5 Hz, CH$_2$), 3.91 (s, 3H, OCH$_3$), 7.31 (d, 1H, J = 8.0 Hz, H-3′), 7.60–7.63 (m, 1H, H-5), 7.65–7.68 (m, 3H, H-6+H-4′ + H6′), 8.20 (d, 1H, J = 8.5 Hz, H-4), 8.27 (d, 1H, J = 8.0 Hz, H-7), 8.61 (s, 1H, CH=N), 12.68 (s, 1H, NH); ^{13}C NMR δ (ppm): 12.36 (CH$_3$), 17.00 (CH$_2$), 52.35 (CH$_2$), 56.26 (OCH$_3$), 113.71 (C-3′), 121.83 (C-6′), 122.99 (C-7), 124.02 (C-4′), 126.97 (C-4), 127.05 (C-5), 127.21 (C-6), 127.93 (C-5′), 136.01 (C-3a), 137.91 (C-1′), 149.10 (C=N), 152.66 (C-7a), 153.11 (C-1′), 156.03 (C-2), 163.65 (C=O); anal. calcd for: C$_{19}$H$_{19}$N$_3$O$_5$S$_2$ (433.50): C, 52.64; H, 4.42; N, 9.69. Found: C, 52.51; H, 4.30; N, 9.84.

3.2. Anti-cancer activity

3.2.1. Cell lines. Characterizations of the three various cancer cell lines used in this study are provided in the ESI† data.

3.2.2. Cell viability assay. The experimental protocol was executed in strict accordance with the methodology previously outlined in ref. 50. Comprehensive supplementary details are available in the accompanying ESI† file.

3.2.3. Determination of IC$_{50}$ values. The ESI† data contains more information.

3.3. Human reactive oxygen species (ROS) estimation

More details are provided in the ESI† data.

3.4. Tubulin beta enzyme-linked immunosorbent assay kit (TUBb)

This experiment was accomplished following the documented procedure.[51] More details are provided in the ESI† data.

3.5. Estimation of DNA fragmentation through DPA assay

DNA fragmentation assessment of the cells was performed according to the reported method.[52] More details are provided in the ESI† data.

3.6. Cell cycle analysis and apoptosis detection

According to the documented procedure employing flow cytometry,[53] cell cycle analysis and apoptosis detection were conducted. More details are provided in the ESI† data.

3.7. Docking

The structural data for the α/β-tubulin heterodimer complexed with nocodazole was retrieved from the Protein Data Bank (PDB entry: 7Z2P). Receptor preparation involved selective chain preservation (A and B), and comprehensive removal of water molecules, ions, and ancillary molecular components. Hydrogen atom modifications included polar hydrogen incorporation and non-polar hydrogen consolidation with corresponding heavy atoms. Kollman charges were systematically applied, and the receptor was subsequently converted to PDBQT format for molecular docking procedures. Compound 6i was graphically rendered using ChemBioDraw Ultra 14.0, underwent energy minimization *via* an MMFF94x Force Field in a gaseous environment, and was formatted to PDBQT. A grid box measuring $20 \times 20 \times 20$ Å with 0.375 Å spacing was positioned centrally on the co-crystallized ligand's coordinates ($X = 16.7$, $Y = 64.9$, $Z = 37.6$). Molecular docking simulation was executed through Autodock 4.2 utilizing default computational parameters. Docking poses were hierarchically ranked based on their computational scores, with the energetically most favorable configuration selected. Interaction analysis and comprehensive visualization were conducted through Discovery Studio Visualizer v21.1.0.20298.[54]

4. Conclusion

The synthesized benzothiazolecarbohydrazide–sulfonate conjugates 6a–l demonstrated reasonable to low cytotoxicity against three distinct human cancer cell lines, and compounds 6e, and 6i showed the highest potency. Meanwhile, compound 6i exhibited no cytotoxicity towards normal cells and showed promising anticancer activity, inducing DNA fragmentation and affecting cell cycle progression in MCF-7 cells. It significantly increased ROS levels, leading to an 8.3-fold rise in DNA fragmentation and a G2 phase increase from 6.85% to 18.27% in MCF-7 cells. Molecular docking indicated a favorable interaction of derivative 6i with the tubulin–colchicine binding site. These findings suggest that benzothiazolecarbohydrazide–sulfonate conjugates, especially compound 6i, hold potential for development as anticancer agents targeting tubulin polymerization. Future studies should focus on detailed mechanistic exploration, *in vivo* efficacy, and optimization to enhance the therapeutic potential.

Data availability

The data supporting this article have been included as part of the ESI.†

Conflicts of interest

There are no conflicts to declare.

Acknowledgements

References

1 C. P. Wild, E. Weiderpass and B. W. Stewart, *World Cancer Report: Cancer Research for Cancer Prevention*, 2020.

2 H. Sung, J. Ferlay, R. L. Siegel, M. Laversanne, I. Soerjomataram, A. Jemal and F. Bray, Global Cancer Statistics 2020: GLOBOCAN Estimates of Incidence and Mortality Worldwide for 36 Cancers in 185 Countries, *Ca-Cancer J. Clin.*, 2021, **71**(3), 209–249, DOI: **10.3322/caac.21660**.

3 I. Soerjomataram and F. Bray, Planning for tomorrow: global cancer incidence and the role of prevention 2020-2070, *Nat. Rev. Clin. Oncol.*, 2021, **18**, 663–672, DOI: **10.1038/s41571-021-00514-z**.

4 I. Jarak, C. L. Varela, E. Tavares da Silva, F. F. M. Roleira, F. Veiga and A. Figueiras, Pluronic-based nanovehicles: Recent advances in anticancer therapeutic applications, *Eur. J. Med. Chem.*, 2020, **206**, 112526–112551, DOI: **10.1016/j.ejmech.2020.112526**.

5 H. H. Fahmy, A. M. Srour, M. A. Ismail, M. A. Khater, R. A. Serrya and M. A. El-Manawaty, Design and synthesis of some new tri-substituted pyrazole derivatives as anticancer agents, *Res. Chem. Intermed.*, 2016, **42**, 6881–6892, DOI: **10.1007/s11164-016-2502-2**.

6 Y. Wan, G. Fang, H. Chen, X. Deng and Z. Tang, Sulfonamide derivatives as potential anti-cancer agents and their SARs elucidation, *Eur. J. Med. Chem.*, 2021, **15**(226), 113837–113858, DOI: **10.1016/j.ejmech.2021.113837**.

7 N. G. Fawazy, S. S. Panda, A. Mostafa, B. M. Kariuki, M. S. Bekheit, Y. Moatasim, *et al.*, Spiro-3-indolin-2-ones: Synthesis, biological properties and computational studies, *Sci. Rep.*, 2022, **12**, 13880–13934, DOI: **10.21203/rs.3.rs-1660054/v1**.

8 A. M. Srour, H. H. Fahmy, M. A. Khater, M. A. El-Manawaty and E. M. Shalaby, Synthesis, characterization, and

cytotoxic activity of some new 1,3,4-trisubstituted pyrazoles against diverse tumor cell lines, *Monatsh. Chem.*, 2018, **149**, 1137–1147, DOI: **10.1007/s00706-018-2153-7**.

9 J. Howard and A. A. Hyman, Dynamics and mechanics of the microtubule plus end, *Nature*, 2003, **422**(6933), 753–758, DOI: **10.1158/1078-0432.CCR-05-2715**.

10 T. E. Hetland, E. Hellesylt, V. A. Flørenes, C. Tropé, B. Davidson and J. Kærn, Class III β-tubulin expression in advanced-stage serous ovarian carcinoma effusions is associated with poor survival and primary chemoresistance, *Hum. Pathol.*, 2011, **42**(7), 1019–1026, DOI: **10.1016/j.humpath.2010.10.025**.

11 R. A. Mohamed-Ezzat and A. M. Srour, Design and Synthesis of Aspirin-chalcone Mimic Conjugates as Potential Anticancer Agents, *Anti-Cancer Agents Med. Chem.*, 2024, **24**(7), 544–557, DOI: **10.2174/0118715206280025231213065519**.

12 P. Lebok, M. Öztürk, U. Heilenkötter, F. Jaenicke, V. Müller, P. Paluchowski, *et al.*, High levels of class III β-tubulin expression are associated with aggressive tumor features in breast cancer, *Oncol. Lett.*, 2016, **11**(3), 1987–1994, DOI: **10.3892/ol.2016.4206**.

13 X. Zhao, C. Yue, J. Chen, C. Tian, D. Yang, L. Xing, *et al.*, Class III β-Tubulin in Colorectal Cancer: Tissue Distribution and Clinical Analysis of Chinese Patients, *Med. Sci. Monit.*, 2016, **22**, 3915–3924, DOI: **10.12659/msm.901252**.

14 G. Ploussard, S. Terry, P. Maillé, Y. Allory, N. Sirab, L. Kheuang, *et al.*, Class III beta-tubulin expression predicts prostate tumor aggressiveness and patient response to docetaxel-based chemotherapy, *Cancer Res.*, 2010, **70**(22), 9253–9264, DOI: **10.1158/0008-5472.CAN-10-1447**.

15 J. Howard and A. A. Hyman, Dynamics and mechanics of the microtubule plus end, *Nature*, 2003, **422**(6933), 753–758, DOI: **10.1038/nature01600**.

16 F. Xu, W. Li, W. Shuai, L. Yang, Y. Bi, C. Ma, *et al.*, Design, synthesis and biological evaluation of pyridine-chalcone derivatives as novel microtubule-destabilizing agents, *Eur. J. Med. Chem.*, 2019, **173**, 1–14, DOI: **10.1016/j.ejmech.2019.04.008**.

17 M. A. Jordan and L. Wilson, Microtubules as a target for anticancer drugs, *Nat. Rev. Cancer*, 2004, **4**(4), 253–265, DOI: **10.1038/nrc1317**.

18 C. Dumontet and M. A. Jordan, Microtubule-binding agents: a dynamic field of cancer therapeutics, *Nat. Rev. Drug Discovery*, 2010, **9**(10), 790–803, DOI: **10.1038/nrd3253**.

19 E. Porcù, R. Bortolozzi, G. Basso and G. Viola, Recent advances in vascular disrupting agents in cancer therapy, *Future Med. Chem.*, 2014, **6**(13), 1485–1498, DOI: **10.4155/fmc.14.104**.

20 S. D. Guggilapu, L. Guntuku, T. S. Reddy, A. Nagarsenkar, D. K. Sigalapalli, V. G. M. Naidu, *et al.*, Synthesis of thiazole linked indolyl-3-glyoxylamide derivatives as tubulin polymerization inhibitors, *Eur. J. Med. Chem.*, 2017, **138**, 83–95, DOI: **10.1016/j.ejmech.2017.06.025**.

21 G. R. Pettit, S. B. Singh, M. R. Boyd, E. Hamel, R. K. Pettit, J. M. Schmidt and F. Hogan, Antineoplastic agents. 291. Isolation and synthesis of combretastatins A-4, A-5, and A-6(1a), *J. Med. Chem.*, 1995, **38**(10), 1666–1672, DOI: **10.1021/jm00010a011**.

22 A. M. Srour, D. H. Dawood and D. O. Saleh, Synthesis, 3D-pharmacophore modelling and 2D-QSAR study of new pyridine-3-carbonitriles as vasorelaxant active agents, *New J. Chem.*, 2021, **45**, 7731–7740, DOI: **10.1039/D0NJ06319C**.

23 A. Irfan, F. Batool, S. A. Zahra Naqvi, A. Islam, S. M. Osman, A. Nocentini, *et al.*, Benzothiazole derivatives as anticancer agents, *J. Enzyme Inhib. Med. Chem.*, 2020, **35**(1), 265–279, DOI: **10.1080/14756366.2019.1698036**.

24 X. H. Shi, Z. Wang, Y. Xia, T. H. Ye, M. Deng, Y. Z. Xu, *et al.*, Synthesis and biological evaluation of novel benzothiazole-2-thiol derivatives as potential anticancer agents, *Molecules*, 2012, **17**(4), 3933–3944, DOI: **10.3390/molecules17043933**.

25 C. O. Leong, M. Suggitt, D. J. Swaine, M. C. Bibby, M. F. Stevens and T. D. Bradshaw, *In vitro*, *in vivo*, and *in silico* analyses of the antitumor activity of 2-(4-amino-3-methylphenyl)-5-fluorobenzothiazoles, *Mol. Cancer Ther.*, 2004, **3**(12), 1565–1575.

26 K. Liu, Y. Ding and C. Kang, Synthesis and Antiproliferative Activity of New N-Acylhydrazone Derivatives Containing Benzothiazole and Indole Based Moiety, *Pharm. Chem. J.*, 2020, **54**, 345–352, DOI: **10.1007/s11094-020-02215-w**.

27 C. G. Mortimer, G. Wells, J. P. Crochard, E. L. Stone, T. D. Bradshaw, M. F. Stevens and A. D. Westwell, Antitumor benzothiazoles. 26.(1) 2-(3,4-dimethoxyphenyl)-5-fluorobenzothiazole (GW 610, NSC 721648), a simple fluorinated 2-arylbenzothiazole, shows potent and selective inhibitory activity against lung, colon, and breast cancer cell lines, *J. Med. Chem.*, 2006, **49**(1), 179–185, DOI: **10.1021/jm050942k**.

28 A. V. S. Rao, B. B. Rao, S. Sunkari, S. P. Shaik, B. Shaik and A. Kamal, 2-Arylaminobenzothiazole-arylpropenone conjugates as tubulin polymerization inhibitors, *MedChemComm*, 2017, **8**, 924–941, DOI: **10.1039/c6md00562d**.

29 D. J. Fu, S. M. Liu, F. H. Li, J. J. Yang and J. Li, Antiproliferative benzothiazoles incorporating a trimethoxyphenyl scaffold as novel colchicine site tubulin polymerisation inhibitors, *J. Enzyme Inhib. Med. Chem.*, 2020, **35**(1), 1050–1059, DOI: **10.1080/14756366.2020.1753721**.

30 N. M. Kumar, S. K. Nukala, T. N. Swamy, M. Ravinder, T. M. Krishna and S. Narsimha, *J. Mol. Struct.*, 2022, **1250**, 131722–131734, DOI: **10.1016/j.molstruc.2021.131722**.

31 S. Grindrod, S. Suy, S. Fallen, M. Eto, J. Toretsky and M. L. Brown, Effects of a fluorescent Myosin light chain phosphatase inhibitor on prostate cancer cells, *Front. Oncol.*, 2011, **1**, 27–44, DOI: **10.3389/fonc.2011.00027**.

32 S. Fortin, X. Charest-Morin, V. Turcotte, C. Lauvaux, J. Lacroix, M. F. Côté, S. Gobeil and R. C-Gaudreault, Activation of Phenyl 4-(2-Oxo-3-alkylimidazolidin-1-yl) benzenesulfonates Prodrugs by CYP1A1 as New

Antimitotics Targeting Breast Cancer Cells, *J. Med. Chem.*, 2017, **60**(12), 4963–4982, DOI: **10.1021/acs.jmedchem.7b00343**.

33 A. B. Krueger, S. J. Dehdashti, N. Southall, J. J. Marugan, M. Ferrer, X. Li, *et al.*, Identification of a selective small-molecule inhibitor series targeting the eyes absent 2 (Eya2) phosphatase activity, *J. Biomol. Screening*, 2013, **18**(1), 85–96, DOI: **10.1177/1087057112453936**.

34 N. W. Gibson, Characterization of DNA damage and cytotoxicity induced in two human colon carcinoma cell lines by cyclodisone, *Cancer Res.*, 1989, **49**(1), 154–157.

35 R. Tamari, M. Scordo, B. M. Kunvarjee, A. Proli, A. Lin, J. Flynn, *et al.*, Association between busulfan exposure and survival in patients undergoing a CD34$^+$ selected stem cell transplantation, *Blood Adv.*, 2023, **7**(18), 5225–5233, DOI: **10.1182/bloodadvances.2023009708**.

36 S. Chen, Y. Zhang, Y. Liu and Q. Wang, Design, Synthesis, Acaricidal Activities, and Structure-Activity Relationship Studies of Novel Oxazolines Containing Sulfonate Moieties, *J. Agric. Food Chem.*, 2019, **67**(49), 13544–13549, DOI: **10.1021/acs.jafc.9b05547**.

37 S. S. Ragab, A. M. Sweed and A. M. Srour, Synthesis and Antiproliferative Properties of Some Spirocyclic Pyrimidine Hydrazones, *ChemistrySelect*, 2024, **9**(8), e202400161, DOI: **10.1002/slct.202400161**.

38 P. Mombelli, M. C. Witschel, A. W. van Zijl, J. G. Geist, M. Rottmann, C. Freymond, *et al.*, Identification of 1,3-Diiminoisoindoline Carbohydrazides as Potential Antimalarial Candidates, *ChemMedChem*, 2012, **7**, 151–158, DOI: **10.1002/cmdc.201100441**.

39 M. Carcelli, D. Rogolino, A. Gatti, M. Sechi, G. Kumar, S. W. White, *et al.*, N-Acylhydrazone inhibitors of influenza virus PA endonuclease with versatile metal binding modes, *Sci. Rep.*, 2016, **6**, 31500–31514, DOI: **10.1038/srep31500**.

40 A. D. Joshi, R. C. Botham, L. J. Schlein, H. S. Roth, A. Mangraviti, A. Borodovsky, *et al.*, Synergistic and targeted therapy with a procaspase-3 activator and temozolomide extends survival in glioma rodent models and is feasible for the treatment of canine malignant glioma patients, *Oncotarget*, 2017, **8**(46), 80124–80138, DOI: **10.18632/oncotarget.19085**.

41 L. P. de Figueiredo, A. L. Ibiapino, D. N. do Amaral, L. S. Ferraz, T. Rodrigues, E. J. Barreiro, *et al.*, Structural characterization and cytotoxicity studies of different forms of a combretastatin A4 analogue, *J. Mol. Struct.*, 2017, **1147**, 226–234, DOI: **10.1016/j.molstruc.2017.06.093**.

42 (*a*) M. A. Omar, R. A. El-Shiekh, D. H. Dawood, A. Temirak and A. M. Srour, Hydrazone-sulfonate hybrids as potential cholinesterase inhibitors: design, synthesis and molecular modeling simulation, *Future Med. Chem.*, 2023, **15**(24), 2269–2287, DOI: **10.4155/fmc-2023-0238**; (*b*) A. F. Kassem, S. S. Ragab, M. A. Omar, N. A. Altwaijry, M. Abdelraof, A. Temirak, A. Saleh and A. M. Srour, New quinazolone-sulfonate conjugates with an acetohydrazide linker as

potential antimicrobial agents: design, synthesis and molecular docking simulations, *RSC Adv.*, 2025, **15**(2), 1033–1048, DOI: **10.1039/d4ra07563c**.

43 A. F. Kassem, M. A. Omar, A. Temirak, R. A. El-Shiekh and A. M. Srour, Barbiturate–sulfonate hybrids as potent cholinesterase inhibitors: design, synthesis and molecular modeling studies, *Future Med. Chem.*, 2024, **16**(16), 1615–1631, DOI: **10.1080/17568919.2024.2366158**.

44 S. Khwaja, K. Kumar, R. Das and A. S. Negi, Microtubule associated proteins as targets for anticancer drug development, *Bioorg. Chem.*, 2021, **116**, 105320–105336, DOI: **10.1016/j.bioorg.2021.105320**.

45 H. Nakamura and K. Takada, Reactive oxygen species in cancer: current findings and future directions, *Cancer Sci.*, 2021, **112**(10), 3945–3952, DOI: **10.1111/cas.15068**.

46 S. J. Kim, H. S. Kim and Y. R. Seo, Understanding of ROS-Inducing Strategy in Anticancer Therapy, *Oxid. Med. Cell. Longevity*, 2019, **2019**, 5381692–5381712, DOI: **10.1155/2019/5381692**.

47 T. Zaidieh, J. R. Smith, K. E. Ball and Q. An, ROS as a novel indicator to predict anticancer drug efficacy, *BMC Cancer*, 2019, **19**(1), 1224–1338, DOI: **10.1186/s12885-019-6438-y**.

48 A. Massarotti, A. Coluccia, R. Silvestri, G. Sorba and A. Brancale, The tubulin colchicine domain: a molecular modeling perspective, *ChemMedChem*, 2012, **7**(1), 33–42, DOI: **10.1002/cmdc.201100361**.

49 W. Li, H. Sun, S. Xu, Z. Zhu and J. Xu, Tubulin inhibitors targeting the colchicine binding site: a perspective of privileged structures, *Future Med. Chem.*, 2017, **9**(15), 1765–1794, DOI: **10.4155/fmc-2017-0100**.

50 M. M. Ibrahim, M. M. Mounier and S. A. Bekheet, Targeting apoptotic anticancer response with natural glucosinolates from cell suspension culture of *Lepidium sativum*, *J. Genet. Eng. Biotechnol.*, 2023, **21**(1), 53–68, DOI: **10.1186/s43141-023-00511-y**.

51 K. Liliom, A. Lehotzky, A. Molnár and J. Ovádi, Characterization of tubulin-alkaloid interactions by enzyme-linked immunosorbent assay, *Anal. Biochem.*, 1995, **228**(1), 18–26, DOI: **10.1006/abio.1995.1309**.

52 K. Burton, A study of the conditions and mechanism of the diphenylamine reaction for the colorimetric estimation of deoxyribonucleic acid, *Biochem. J.*, 1956, **62**(2), 315–323, DOI: **10.1042/bj0620315**.

53 S. Diab, T. Teo, M. Kumarasiri, P. Li, M. Yu, F. Lam, *et al.*, Discovery of 5-(2-(phenylamino)pyrimidin-4-yl)thiazol-2(3H)-one derivatives as potent Mnk2 inhibitors: synthesis, SAR analysis and biological evaluation, *ChemMedChem*, 2014, **9**(5), 962–972, DOI: **10.1002/cmdc.201300552**.

54 M. A. Raslan and A. H. Afifi, *In vitro* wound healing properties, antioxidant activities, HPLC-ESI-MS/MS profile and phytoconstituents of the stem aqueous methanolic extract of *Dracaena reflexa* Lam, *Biomed. Chromatogr.*, 2022, **36**(6), e5352, DOI: **10.1002/bmc.5352**.